

1 **S1: Estimation of hurricane wind speed at BEW**

2 Hurricane wind field can be reconstructed using the HURRECON model, which estimates sustained wind speed, peak
3 gust, and wind direction at a given point using the information of the track, size, and intensity of a hurricane and the
4 cover type (land or water) of the point (Boose et al. 1994; Boose et al. 2004). The sustained wind speed (V_s ; m s^{-1}) at
5 any point P in the northern hemisphere are estimated as

$$V_s = F \left[V_m - \frac{1}{2} S (1 - \sin(T)) V_h \right] \times \sqrt{\left(\frac{R_m}{R} \right)^B \exp \left(1 - \left(\frac{R_m}{R} \right)^B \right)}, \quad (\text{S1})$$

6 where F is the scaling parameter for friction ($F = 1$ if point P is on water, 0.8 otherwise), S is the scaling parameter
7 for hurricane asymmetry (1.0), V_m is the maximum overwater sustained wind speed (m s^{-1}) of the hurricane, T is the
8 clockwise angle (degree) between the direction of the hurricane movement and the direction from hurricane center to
9 point P , V_h is the velocity (m s^{-1}) of the hurricane movement, R is the distance (km) from hurricane center to point P ,
10 R_m is the radius of maximum winds (20-80 km), and B is the scaling parameter controlling the shape of the wind
11 profile curve (1.2-1.5).

12 We estimate the tropical cyclones ($39 \text{ mph} \leq \text{sustained wind} < 73 \text{ mph}$) that passed near BEW within 100
13 km or hurricanes ($\geq 74 \text{ mph}$) that passed within 150 km of BEW between 1989 and 2017 (the period of the BEW
14 censuses) using the HURRECON model. The hurricane best track data HURDAT2 (Landsea and Franklin 2013) are
15 used for parameters F , S , V_m , T , V_h , and R ; and we assume that the maximum wind radius $R_m = 30 \text{ km}$ and the scale
16 parameter of the shape of the wind profile curve $B = 1.5$ for all tropical storms (cyclones and hurricanes) for
17 convenience.

18 **S2: Estimation of non-photosynthetic vegetation at BEW**

19 Non-photosynthetic vegetation (NPV) data derived from satellite remote sensing retrievals are used to quantify the
20 forest damage from hurricane disturbances. NPV includes exposed wood and surface litter and represents dead
21 vegetation. NPV, together with photosynthetic vegetation (PV, also called green vegetation) and bare soil (BS) are the
22 three main ground cover types. NPV, PV, and BS have distinct spectral reflectance at visible and infrared spectrums,
23 and thus they can be distinguished by satellite sensors with multiple spectral bands. However, satellites cannot
24 distinguish different ground cover types when a grid pixel is a mixture of the three. For each grid pixel, the spectral
25 reflectance measured by satellites (R_λ) is the average of the spectral reflectance of each ground cover type ($M_{type, \lambda}$),
26 weighted by their fractional cover (f_{type}):

$$R_\lambda = f_{NPV} M_{NPV, \lambda} + f_{PV} M_{PV, \lambda} + f_{BS} M_{BS, \lambda}, \quad (\text{S2})$$

27 where λ is the wavelength band at which satellite detects signals. The fractional cover of each ground cover type is
28 bounded by two constraints: 1) non-negativity constraint $f_{type} \geq 0$, and 2) sum-to-one constraint $f_{NPV} + f_{PV} + f_{BS} = 1$.

29 To obtain the fractional cover of each ground cover types, we use the surface reflectance data (R_λ) from
30 Landsat satellites from USGS (<https://landsat.gsfc.nasa.gov/>). Landsat 4 and 5 satellites provide natural color images

31 and surface reflectance at six wavelength bands—three in visible spectrum (0.45-0.52 μm , 0.52-0.60 μm , and 0.63-
 32 0.69 μm), one in near infrared spectrum (0.76-0.90 μm), and two in short-wavelength infrared spectrum (1.55-1.75
 33 μm and 2.08-2.35 μm)—from 1982 to 1992 (Landsat 5 continued to operate until 2012 but no data available). Landsat
 34 7 provides the same information since 1999. Landsat 8 (launched in 2013) provides the same information since 2015
 35 but with slightly narrower ranges of each band (0.45-0.515 μm , 0.525-0.60 μm , 0.63-0.68 μm , 0.845-0.885 μm , 1.56-
 36 1.66 μm , and 2.1-2.3 μm). The surface reflectance data have a 30-m spatial resolution and a 16-day temporal
 37 resolution, but cloud cover significantly reduces the availability of high-quality surface reflectance data.

38 The spectral reflectance of the three ground covers ($M_{type, \lambda}$) are derived from the satellite surface reflectance
 39 at each spectral band for three boxed areas in Puerto Rico on June 6 and October 12, 2017 (Figure S13). The three
 40 boxed areas correspond to dense forest, disturbed forest, and bare ground according to the natural color images from
 41 Landsat satellites (Figure S13) and thus represent the ground cover types of PV, NPV, and BS, respectively. The
 42 spectral reflectance of the three ground cover types generally agrees with previous results (Yang et al. 2012; Li et al.
 43 2017). It shows that bare soil has the largest reflectance at all the six wavelength bands compared with NPV and PV.
 44 PV has a large reflectance on the near infrared ($\sim 0.84\mu\text{m}$) band but small reflectance on visible (0.4–0.7 μm) and short-
 45 wavelength infrared ($\sim 1.65\mu\text{m}$ and $\sim 2.21\mu\text{m}$) bands.

46 To obtain the fractional cover of each type (f_{type}), we use the bounded variable least square method following
 47 Lawson and Hanson (1974) and Guerschman et al. (2015). Equation (S2) changes to

$$[\mathbf{R}, \delta] = \mathbf{f}[\mathbf{M}, \delta \mathbf{1}^m], \quad (\text{S3})$$

48 where \mathbf{R} is a $1 \times n$ dimensional vector of satellite reflectance and n is number of wavelength bands ($n=6$), \mathbf{f} is a $1 \times m$
 49 dimensional vector of the fractional cover and m is the number of ground cover types ($m=3$), \mathbf{M} is an $m \times n$ dimensional
 50 matrix of the spectral reflectance of each ground cover type, and δ is a weighting for the sum-to-one constraint and $\mathbf{1}^m$
 51 is the $m \times 1$ vector with all elements being 1. The value of δ is set to 0.2 following Guerschman et al. (2015). Then
 52 the fractional cover \mathbf{f} is obtained as

$$\mathbf{f} = \min_{\mathbf{f}} \|\mathbf{f}[\mathbf{M}, \delta \mathbf{1}^m] - [\mathbf{R}, \delta]\|_2^2, \text{ where } \mathbf{f} \geq 0, \quad (\text{S4})$$

53 using the embedded function *lsqnonneg* in MATLAB. Thus, the fractional cover of NPV (f_{NPV}) for Puerto Rico is
 54 obtained whenever surface reflectance data are available.

55 ΔNPV is calculated as the difference of NPV between two dates, one before a hurricane and one after the
 56 hurricane. The revisit time of Landsat satellites is 16 days, but not all data are available or with high quality because
 57 of heavy cloud coverage. Therefore, the pre-hurricane and post-hurricane dates are those closest to the hurricane with
 58 high-quality Landsat satellite data (Table S2). The pre-hurricane and post-hurricane dates are usually within a month
 59 of the hurricane, and some are three or four months apart. Note that the pre-Hugo date (November 1988) is 10 months
 60 before hurricane Hugo (September 1989), the post-Earl date (April 2011) is eight months after hurricane Earl (August
 61 2010), and the dates for hurricanes Marilyn (1995), Bertha (1996), and Georges (1998) are not available because there
 62 were no Landsat data available between September 1992 and August 1999. The ΔNPV calculated from two dates, pre-
 63 and post-hurricane dates, that are several months apart may be biased and may not reflect the accurate change of NPV
 64 from the hurricane due to the seasonal variation of the NPV. Nevertheless, ΔNPV of a hurricane estimated here
 65 provides preliminary and approximate information of the mortality of the hurricane.

66 Figure S14 shows ΔNPV after each hurricane since 1989 with a trajectory close to BEW. Due to heavy cloud
 67 coverage, the ΔNPV in many grid pixels is not available. The figure shows that consecutive hurricanes in the same
 68 year (i.e., hurricanes Jose and Lenny in 1999, hurricanes Irma and Maria in 2017) caused severer damages (higher
 69 ΔNPVs) than a single hurricane. Note that the ΔNPV of hurricane Irene is negative for most of the pixels, indicating
 70 decrease of NPV and thus increase of greenness, which is possibly not reflecting the true ΔNPV directly caused by
 71 the hurricane. The pre-hurricane date for Irene is April 11 (Table S2), green vegetation could accumulate in the
 72 growing season and the fractional coverage of NPV would decrease when hurricane Irene hits on August 22, 2011.
 73 Therefore, the NPV before hurricane Irene was possibly overestimated and thus the ΔNPV underestimated.

74 **S3: The relationship between forest mortality and hurricane wind speed**

75 The relationship between the rate of forest mortality and local hurricane wind speed has been studied through an
 76 intermediate variable: the fractional coverage of non-photosynthetic vegetation (NPV). The difference of NPV
 77 (ΔNPV) before and after a hurricane is indicative of tree mortality. Specifically, negative value indicates decrease of
 78 NPV and thus the increase of greenness, positive value indicates increase of NPV and thus mortality, and higher
 79 positive ΔNPV indicates higher mortality (Chambers et al. 2007; Negrón-Juárez et al. 2010; Negrón-Juárez et al.
 80 2014). However, the relationship between ΔNPV and wind speed is site sensitive (Chambers et al. 2007; Zeng et al.
 81 2009; Negrón-Juárez et al. 2010; Negrón-Juárez et al. 2014). Therefore, we use ΔNPV to qualitatively represent the
 82 forest mortality after hurricane disturbances at BEW.

83 Figure S15 shows the scatter plot of the average ΔNPV over the $40\text{km} \times 40\text{km}$ area centered at BEW (blue
 84 boxes in Figure S14) after each hurricane against the corresponding wind speed at BEW. It shows ΔNPV is
 85 approximately 0.3 after hurricane Hugo and approximately 0.6 after consecutive hurricanes Irma and Maria. Hurricane
 86 Irma did not cause direct mortality to the forest, but it removed a significant amount of foliage (Uriarte et al. 2019)
 87 and saturated the soils and loosened the roots (Hall et al. 2020), making trees more vulnerable when hurricane Maria
 88 came. Thus, we believe the mortality caused by Maria was aggravated because of hurricane Irma. The ΔNPV is around
 89 zero for all other hurricanes, which means that those hurricanes do not significantly change the fractional cover of
 90 NPV. Therefore, a binary relationship between ΔNPV and local wind speed is suggested:

$$\Delta\text{NPV} = \begin{cases} 0, & V < V_0 \\ \Delta\text{NPV}_0, & V \geq V_0 \end{cases} \quad (\text{S5})$$

91 ΔNPV_0 varies with forest state and other factors. The threshold V_0 is set to 41 m s^{-1} because, based on census data and
 92 meteorological records, the largest local wind speed that caused no mortality in BEW is 40 m s^{-1} corresponding to
 93 hurricane Georges and the smallest wind speed that caused mortality in the forest is 42 m s^{-1} corresponding to hurricane
 94 Maria. Since ΔNPV is indicative of forest mortality (Chambers et al. 2007; Negrón-Juárez et al. 2010; Negrón-Juárez
 95 et al. 2014), we assume that hurricane strength has the same binary effect on forest mortality.

96

97 **Supplementary Tables**

98 **Table S1.** Values of allometric parameters for each PFT.

Parameter Name	Units	Early	Mid	Late	Palm
H-DBH scale parameter (a in Eq. (1))	m cm ⁻¹	1.6388	2.2054	2.3833	0.1628
H-DBH shape parameter (b in Eq. (1))	-	0.80	0.64	0.59	1.47
Allocation to reproduction	proportion	0.3	0.3	0.3	1
Reproduction min. height	m	18	18	18	18
Minimum height	m	1.5	1.5	1.5	4.8

99

100

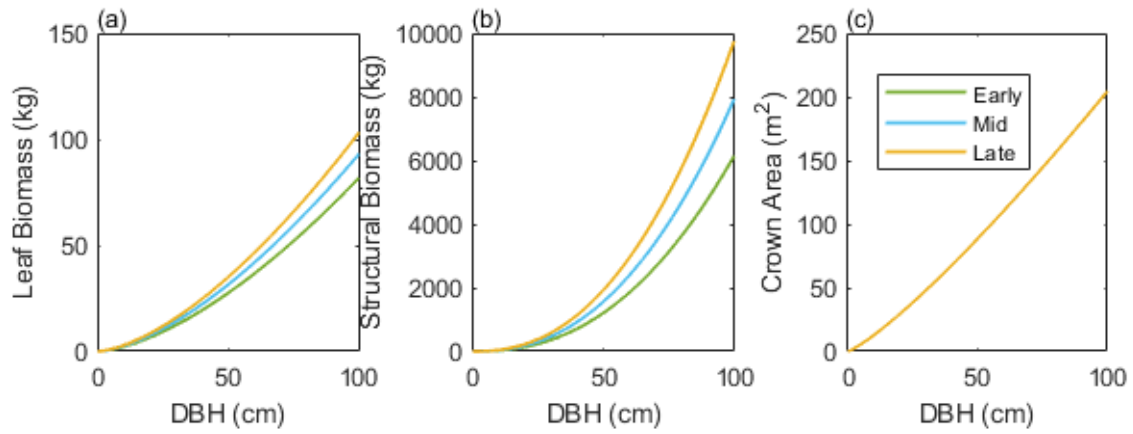
101 **Table S2.** The pre- and post-hurricane dates that are used for calculating Δ NPV for each hurricane. The pre- and post-hurricane
 102 dates for Marilyn, Bertha, and Georges are not available because there were no Landsat data in those years. For some hurricanes,
 103 the pre- (post-) hurricane dates are months before (after) the hurricane date because there were no high-quality satellite data
 104 available for closer dates due to heavy cloud coverage.

Hurricane Name	Hurricane Date (yyyy-mm-dd)	Pre-hurricane date	Post-hurricane date
Hugo	1989-09-18	1988-11-05	1989-10-07
Marilyn	1995-09-16	---	---
Bertha	1996-07-08	---	---
Georges	1998-09-21	---	---
Jose & Lenny	1999-10-21 1999-11-17	1999-09-17	2000-03-27
Debby	2000-08-22	2000-08-02	2001-01-09
Dean	2001-08-22	2001-07-20	2002-04-02
Jeanne	2004-09-15	2004-08-29	2004-10-16
Olga	2007-12-11	2007-09-23	2008-02-14
Earl	2010-08-31	2010-05-10	2011-04-11
Irene	2011-08-22	2011-04-11	2011-09-02
Irma & Maria	2017-09-07 2017-09-20	2017-06-06	2017-10-12

105

106

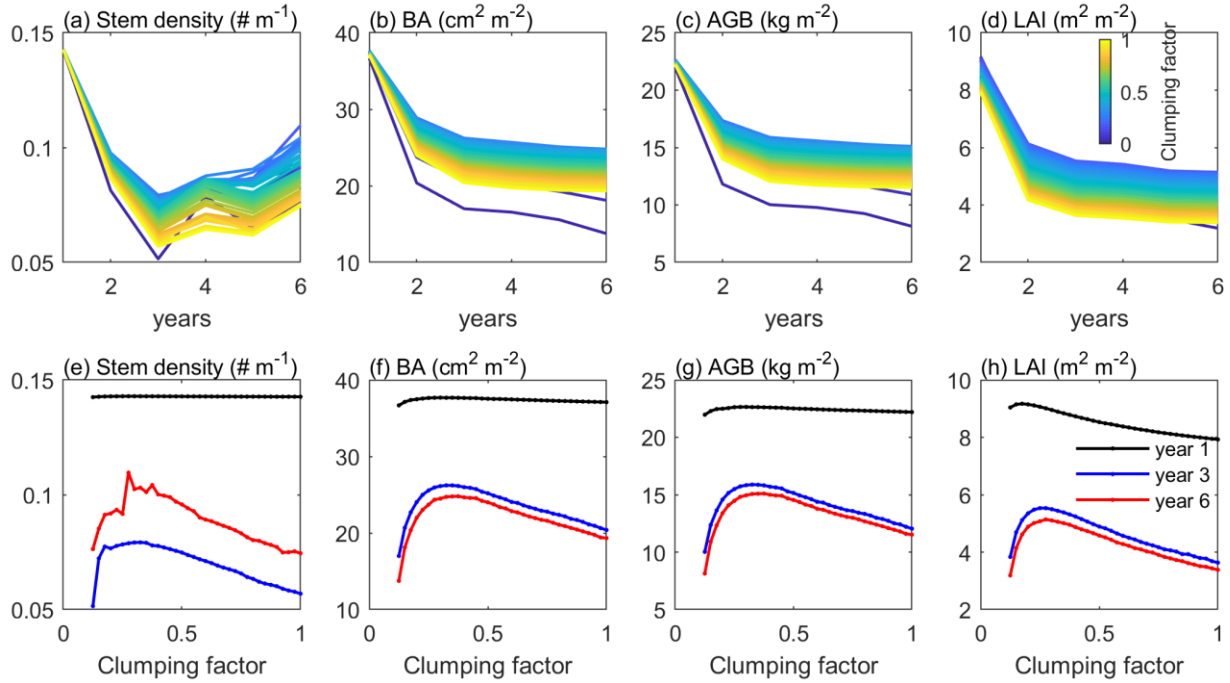
107 **Supplementary Figures**



108

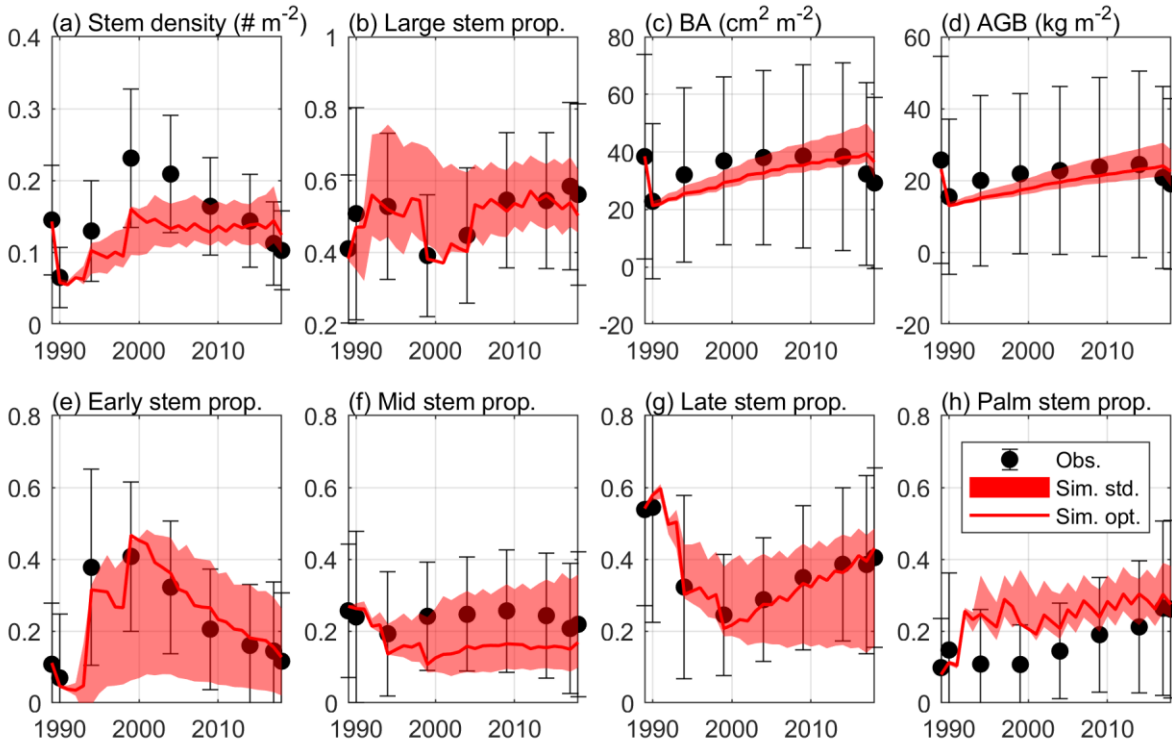
109 **Figure S1.** The ED2 model default allometries for each PFT (Early, Mid, and Late tropical successional trees). (a) Leaf biomass-
110 DBH allometry, (b) structural biomass-DBH allometry, and (c) crown area-DBH allometry. The allometries for Palm PFT is
111 assumed the same as those for Early PFT.

112



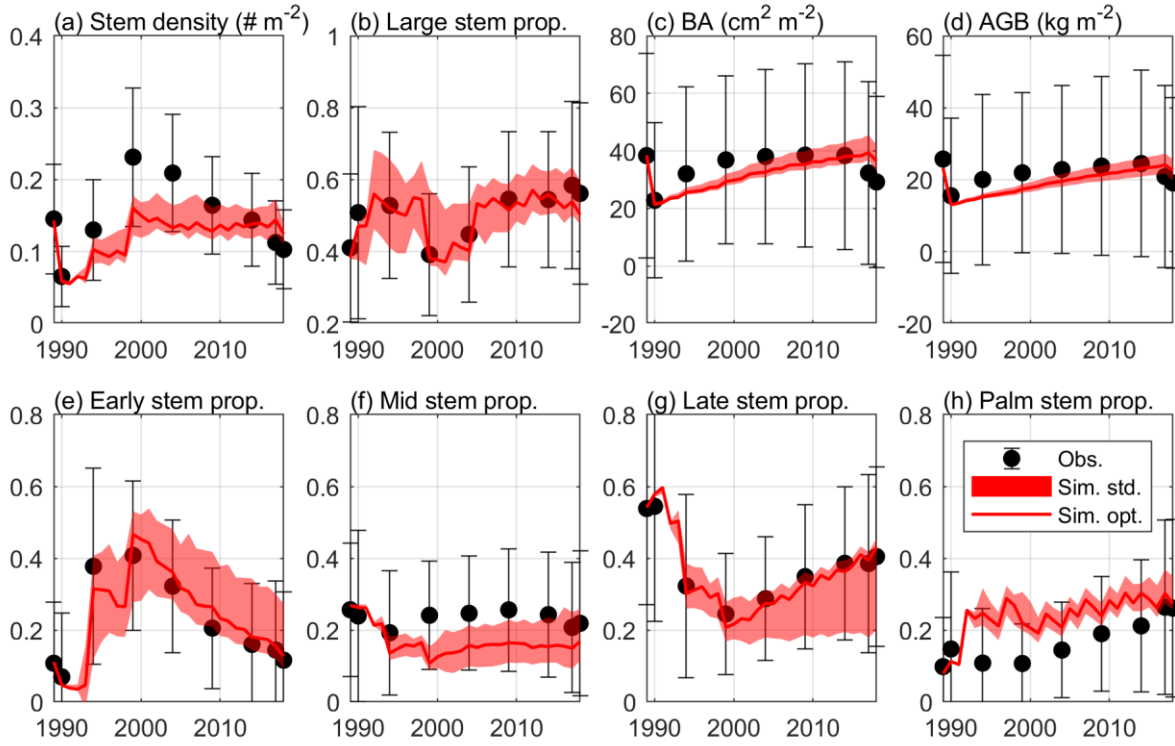
113
 114 **Figure S2.** Time series of (a) stem density, (b) basal area, (c) aboveground biomass, and (d) leaf area index for different values of
 115 the parameter leaf clumping factor. (e)-(h) The values of the variables at the first, third, and sixth simulation years.

116



117
 118 **Figure S3.** Same as Figure 4, but for $K=6$.

119

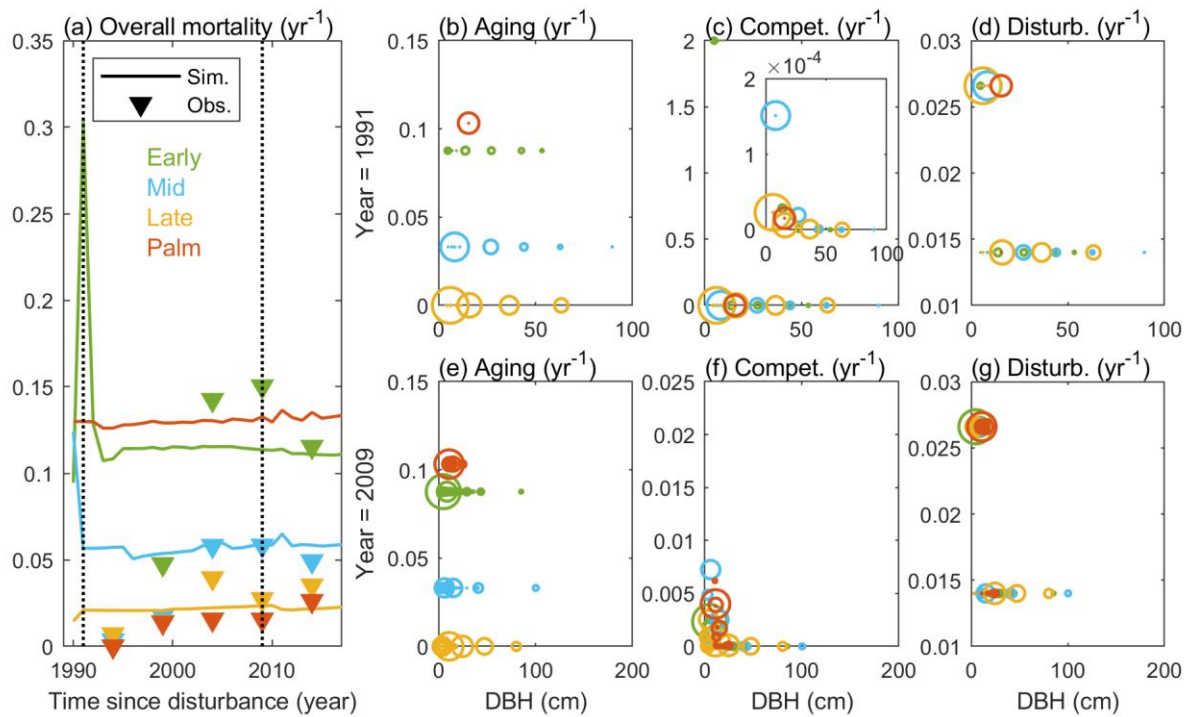


120

121 **Figure S4.** Same as Figure 4, but for $K=10$.

122

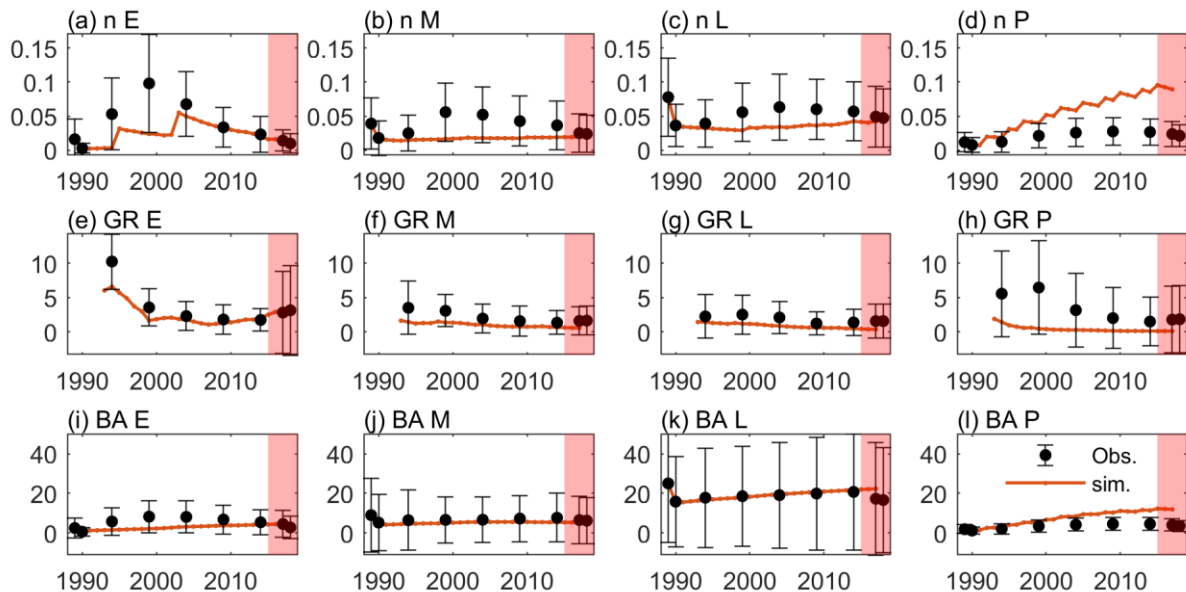
123



124

125 **Figure S5.** Mortality for each PFT. (a) The time series of the simulated and observed overall mortality for the four PFTs: Early,
 126 Mid, Late, and Palm. The simulated mortality from (b) aging, (c) competition, and (d) disturbance for each cohort in year 1991. X-
 127 axes are the DBH of the cohort, the color of the circle represents the PFT of the cohort, and the size of the circle is proportional to
 128 the density of the cohort (individuals m⁻²). (e)-(g) are the same as (b)-(d), but for year 2009.

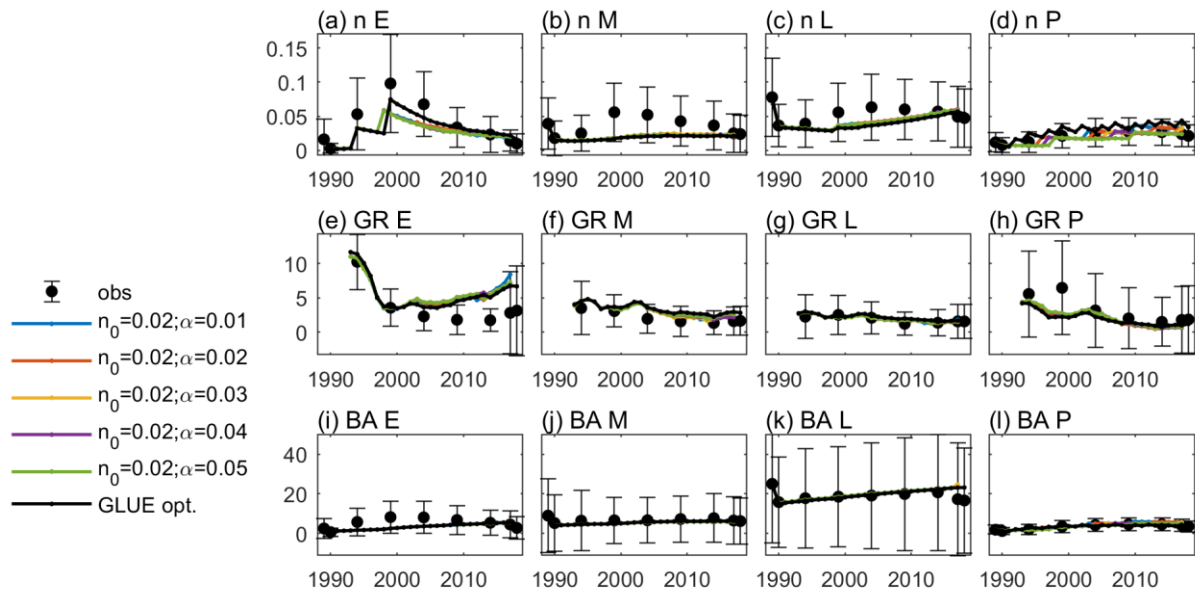
129



130

131 **Figure S6.** Same as Figure 3, but the model results are from the simulation with the aging mortality of Palm set to zero.

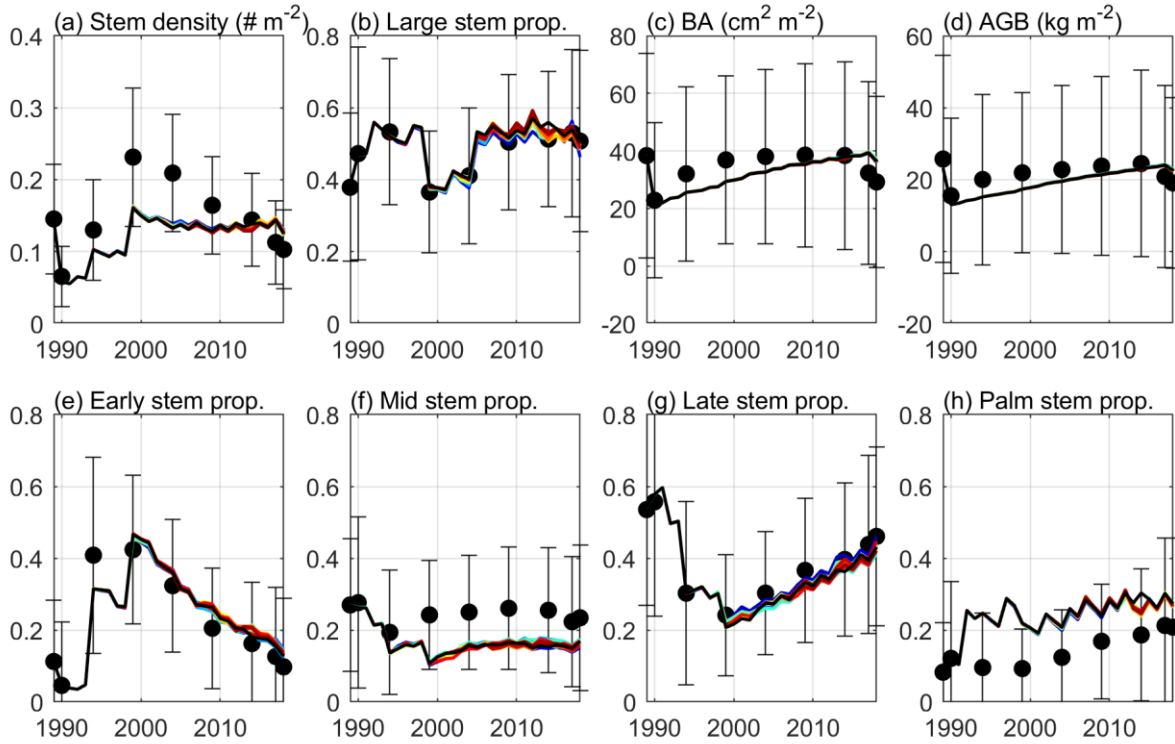
132



133

134 **Figure S7.** Same as Figure 3, but the optimal simulation is shown in black, and colored lines show experiments with 0 aging
 135 mortality and different seedling densities of Palm.

136



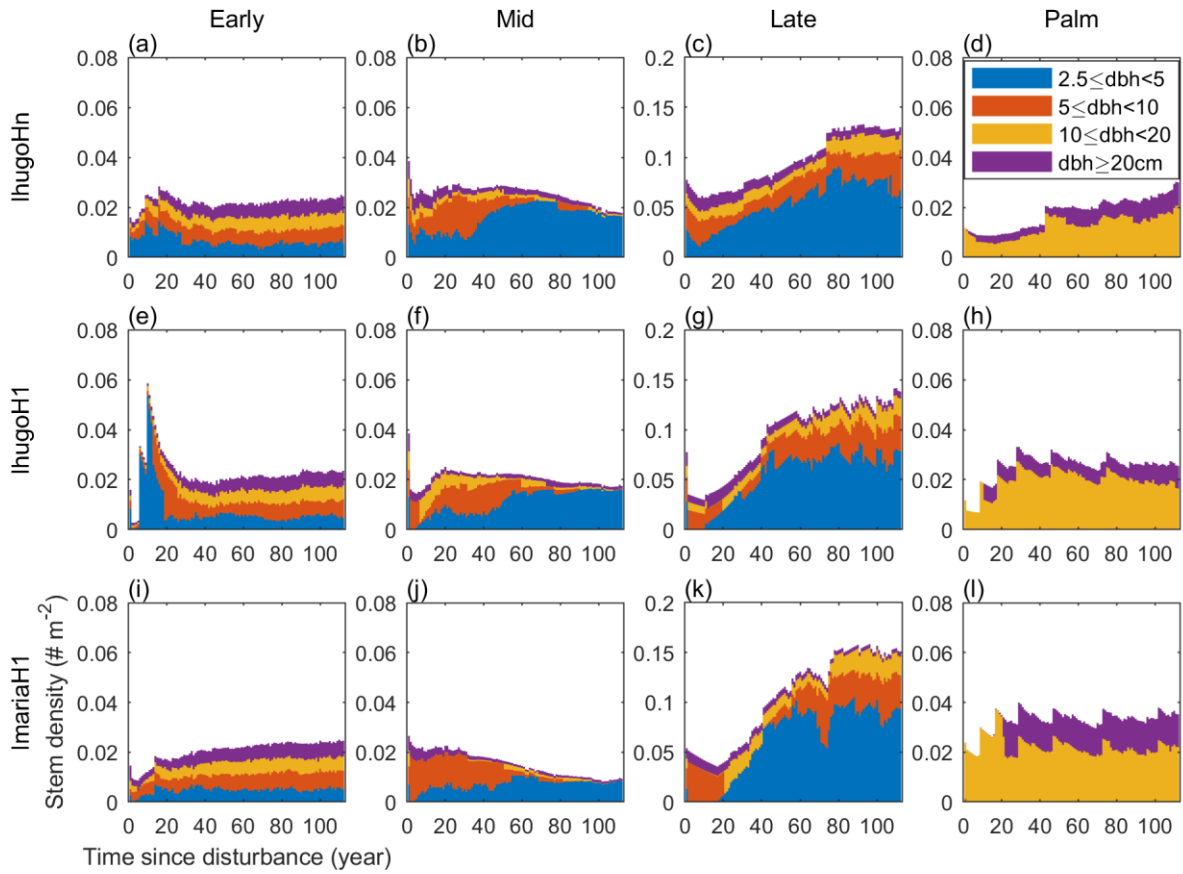
137

138

139

Figure S8. Same as Figure 4, but the optimal simulation is shown in black, and colored lines show the top 20 parameter sensitivity experiments with smaller *MSE* than the optimal simulation.

140

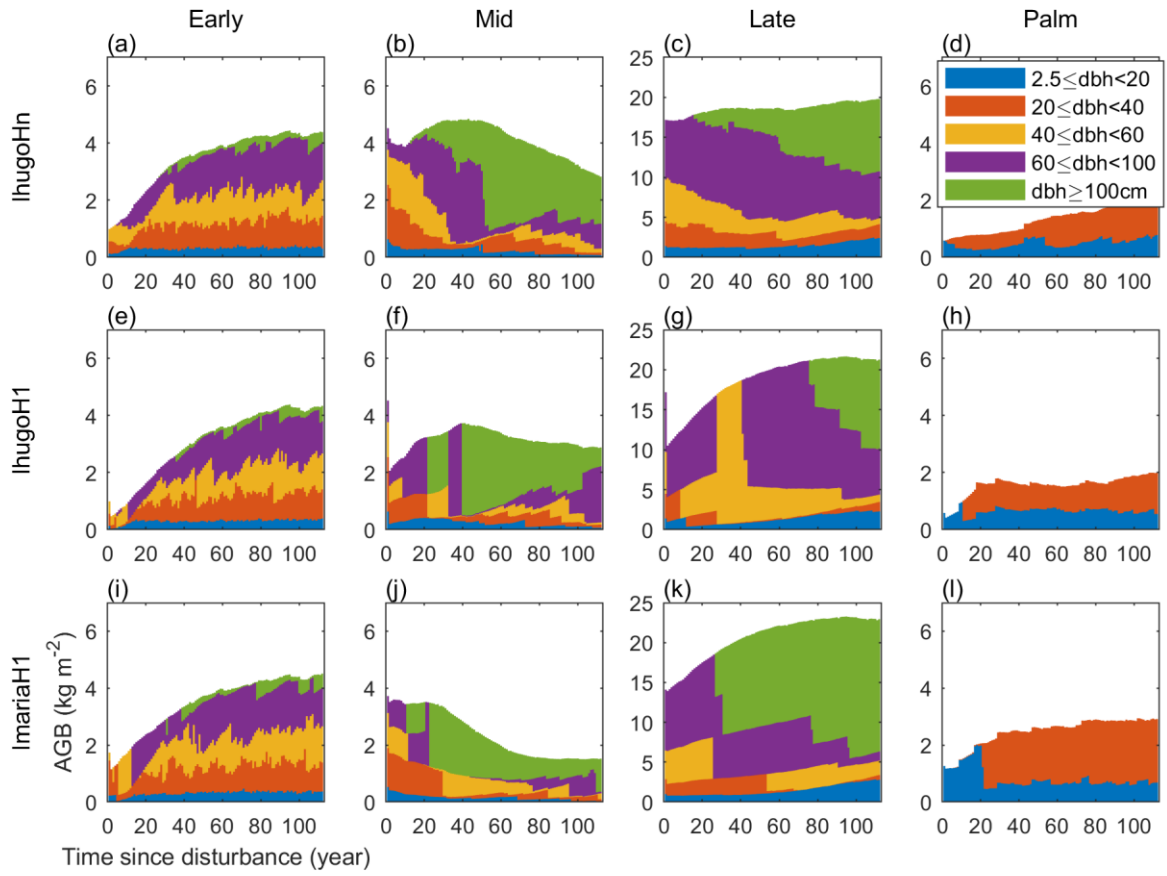


141

142

Figure S9. Time series of the distribution of DBHs for the stem density of each PFT from the three experiments.

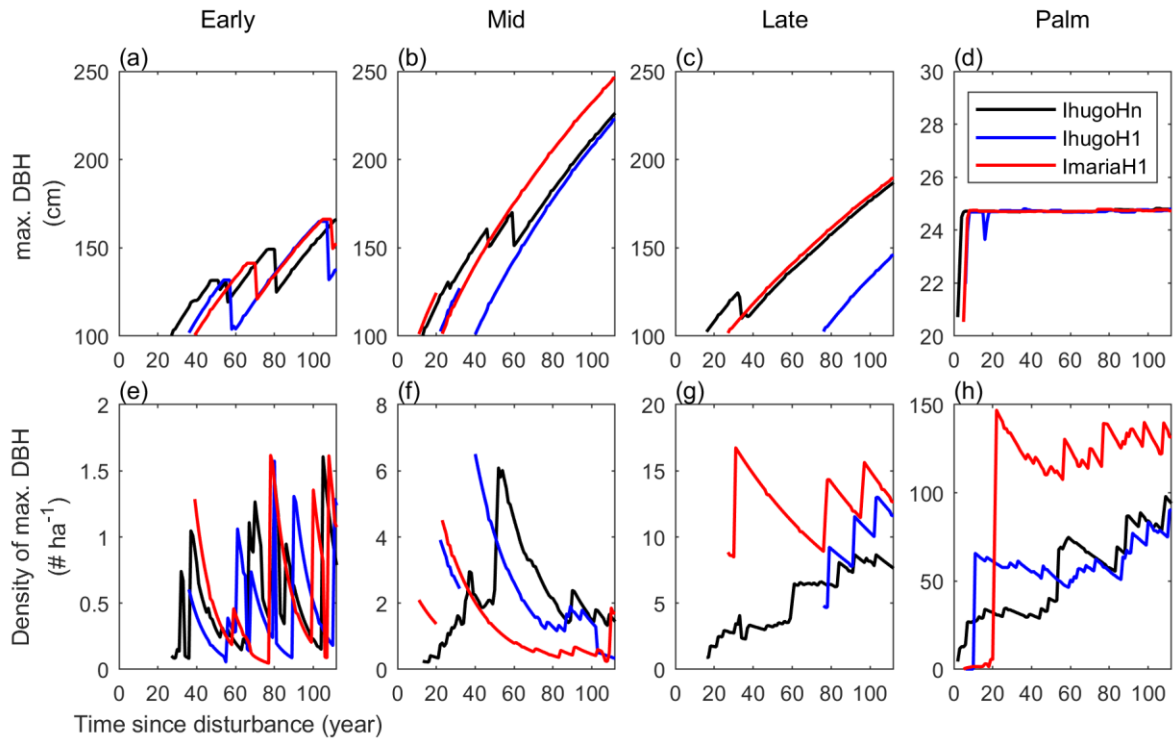
143



144

145 **Figure S10.** Time series of the distribution of DBHs for AGB of each PFT from the three experiments.

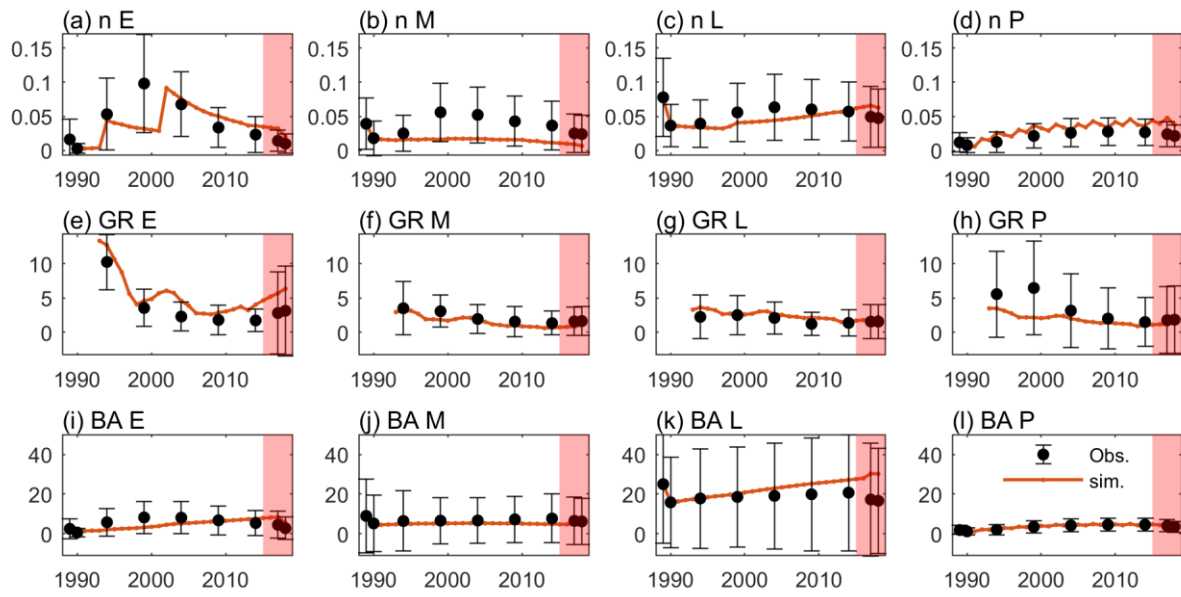
146



147

148 **Figure S11.** Time series of the maximum DBH and the density of the largest DBH class (DBH \geq 100 cm for Early, Mid, and Late
 149 PFTs, and $20 \leq$ DBH < 25 cm for Palm) for each PFT from the three experiments.

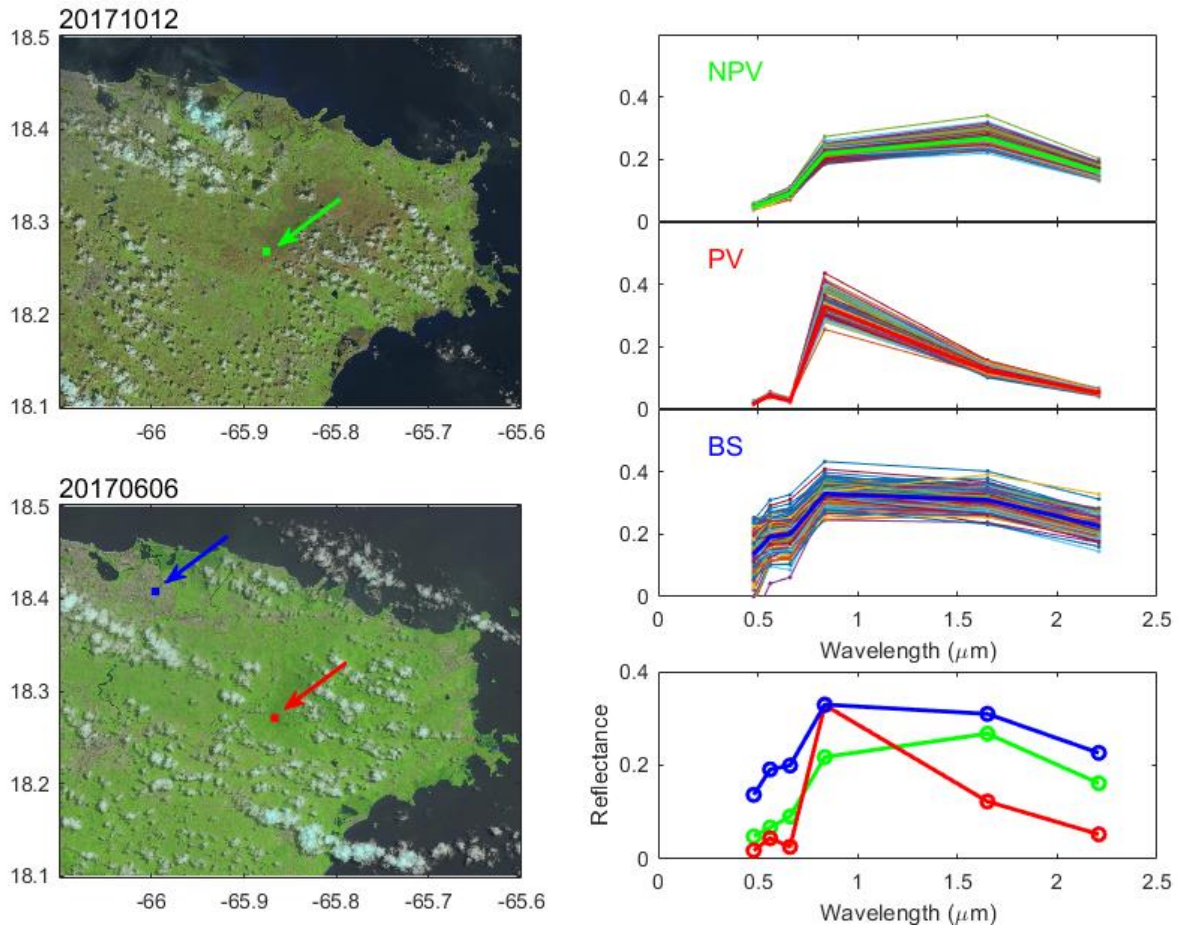
150



151

152 **Figure S12.** Same as Figure 3, except that the sample size for GLUE is 20,000.

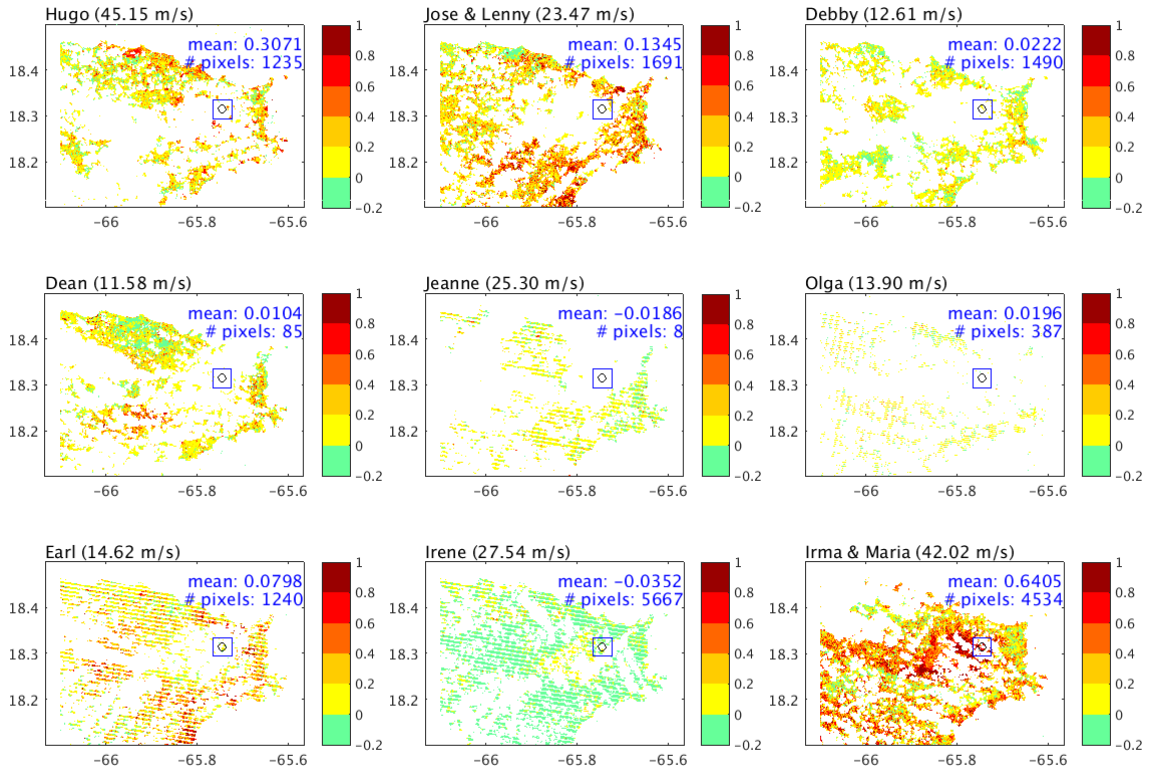
153



154

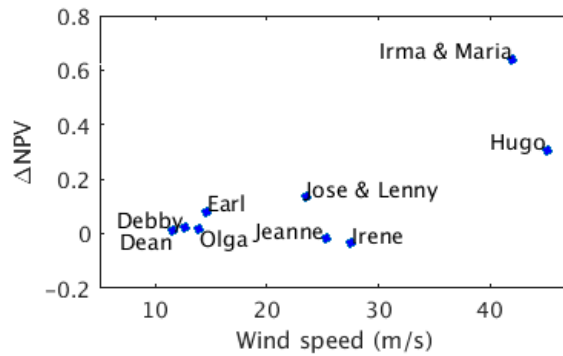
155 **Figure S13.** Reflectance of each ground cover type (NPV, PV, and BS) at six wavelengths in the visible and infrared spectrum.
 156 The left two panels are the natural color images of two dates. The right panels show the spectral reflectance of the three landcovers.
 157 The spectral reflectance of NPV is obtained from the reflectance of a 500m-by-500m spatial domain (about 200 pixels) on October
 158 12, 2017 (green box in the upper left panel), and the those of PV and BS are from the same sized domain on June 6, 2017 (red and
 159 blue boxes on the lower left panel).

160



161
 162 **Figure S14.** The spatial distribution of Δ NPV over the northeastern Puerto Rico for each hurricane. The name of each hurricane
 163 and the corresponding maximum wind speed at BEW are shown on the upper left of each panel. The second and the last panels
 164 show Δ NPV after two consecutive hurricanes and the wind speed of the stronger one is given in the parenthesis. Pixels over water
 165 or covered by clouds are shown in white. The black circle indicates the location of BEW (-65.7449 W; 18.3144 N), and the blue
 166 box is 4km-4km area centered at BEW. The number of pixels inside the box that have Δ NPV value and the mean value of Δ NPV
 167 inside the box are shown for each panel.

168



169
 170 **Figure S15.** Scatter plot of Δ NPV against the corresponding wind speed at BEW for each hurricane shown in Figure S14.

171

172 **References**

- 173 Boose, E. R., Foster, D. R., and Fluet, M.: Hurricane Impacts of tropical and temperate forest landscapes, *Ecological*
174 *Monographs*, 64, 369–400, 1994.
- 175 Boose, E. R., Serrano, M. I., and Foster, D. R.: Landscape and regional impacts of hurricanes in Puerto Rico,
176 *Ecological Monographs*, 74, 335–352, 2004.
- 177 Guerschman, J. P. et al.: Assessing the effects of site heterogeneity and soil properties when unmixing photosynthetic
178 vegetation, non-photosynthetic vegetation and bare soil fractions from Landsat and MODIS data, *Remote*
179 *Sensing of Environment*, 161, 12–26 2015.
- 180 Landsea, C. W. and Franklin, J. L.: Atlantic Hurricane Database Uncertainty and Presentation of a New Database
181 Format, *Month Weather Review*, 141, 3576–3592, 2013.
- 182 Lawson, C. L. and Hanson, R. J.: *Solving Least-Squares Problems*, Upper Saddle River, NJ: Prentice Hall. Chapter
183 23, p. 161, 1974.
- 184 Li, X. et al.: A 2001–2015 Archive of fractional cover of photosynthetic and non-photosynthetic vegetation for Beijing
185 and Tianjin Sandstorm Source Region, *Data*, 2, 27, 2017.
- 186 Negrón-Juárez, R. I. et al.: Widespread amazon forest tree mortality from a single cross-basin squall line event,
187 *Geophysical Research Letters*, 37, L16701, 2010.
- 188 Negrón-Juárez, R., Baker, D. B., Chambers, J. Q., Hurtt, G. C., and Goosem, S.: Multi-scale sensitivity of Landsat
189 and MODIS to forest disturbance associated with tropical cyclones, *Remote Sensing of Environment*, 140,
190 679–689, 2014.
- 191 USGS, 1/3-Arc Second National Elevation Dataset, US Geological Survey, Reston, VA. 2018.
- 192 Yang, J., Weisberg, P. J., and Bristow, N. A.: Landsat remote sensing approaches for monitoring long-term tree cover
193 dynamics in semi-arid woodlands: Comparison of vegetation indices and spectral mixture analysis, *Remote*
194 *Sensing of Environment*, 119, 62–71, 2012.
- 195 Zeng, H., Chambers, J. Q., Negrón-Juárez, R. I., Hurtt, G. C., Baker, D. B., and Powell, M. D.: Impacts of tropical
196 cyclones on U.S. forest tree mortality and carbon flux from 1851 to 2000, *Proceedings of the National*
197 *Academy of Sciences of the United States of America*, 106, 7888–7892, 2009.
- 198